HHS Public Access

Author manuscript

Small. Author manuscript; available in PMC 2021 May 01.

Published in final edited form as:

Small. 2020 May ; 16(21): e2000303. doi:10.1002/smll.202000303.

Chemical and Colloidal Dynamics of MnO_2 Nanosheets in Biological Media Relevant for Nanosafety Assessment

Evan P. Gray[†],
Civil Environmental and Construction Engineering Department, Texas Tech University, 79409, USA

Cynthia L. Browning[†],
Department for Pathology and Laboratory Medicine, Brown University, Providence RI 02912

Charles A. Vaslet,
Department for Pathology and Laboratory Medicine, Brown University, Providence RI 02912

Kyle D. Gion,
The School of Engineering, Brown University, Providence RI, 02912

Allen Green,
The School of Engineering, Brown University, Providence RI, 02912

Muchun Liu,
Department of Chemistry, Brown University, Providence RI, 02912

Agnes B. Kane,
Department for Pathology and Laboratory Medicine, Brown University, Providence RI 02912

Robert H. Hurt
The School of Engineering Brown University, Providence RI, 02912

Abstract

Many layered crystal phases can be exfoliated or assembled into ultrathin two-dimensional (2D) nanosheets with novel properties not achievable by particulate or fibrous nanoforms. Among these 2D materials are manganese dioxide (MnO_2) nanosheets, which have applications in batteries, catalysts, and biomedical probes. A novel feature of MnO_2 is its sensitivity to chemical reduction leading to dissolution and Mn^{2+} release. Biodissolution is critical for nanosafety assessment of 2D materials, but the timing and location of MnO_2 biodissolution in environmental or occupational exposure scenarios are poorly understood. This work investigates the chemical and colloidal dynamics of MnO_2 nanosheets in biological media for environmental and human health risk assessment. MnO_2 nanosheets are insoluble in most aqueous phases, but react with strong and weak reducing agents in biological fluid environments. In vitro, reductive dissolution can be slow

[*]corresponding authors: Robert_Hurt@brown.edu, Agnes_Kane@brown.edu.
[†]Authors contributed equally

Supporting Information
Supporting Information is available from the Wiley Online Library or from the author.

Conflict of Interest
The authors declare no conflict of interest.

enough in cell culture media for MnO_2 internalization by cells in the form of intact nanosheets, which localize in vacuoles, react to deplete intracellular glutathione, and induce cytotoxicity that is likely mediated by intracellular Mn^{2+} release. The results are used to classify MnO_2 nanosheets within a new hazard screening framework for 2D materials, and the implications of MnO_2 transformations for nanotoxicity testing and nanosafety assessment are discussed.

Keywords

2D materials; manganese dioxide; biodissolution; exposure; nanosafety

1. Introduction

As we enter a new decade, it may be appropriate to reflect on progress in the field that we now refer to as "nanosafety".[1,2] Over 15 years of intensive research has taken place in academic, government, and industry laboratories, on hundreds of different nanomaterials, and covering aspects of this complex issue that include nanomaterial release, environmental fate and transport, material transformations, exposure, safe design,[2–4] and biological responses[1,5,6] from a wide array of in vitro and in vivo model systems.[7] This work has provided a wealth of scientific information that has guided policy and regulation,[8,9] and helped distinguish real risks from the many potential risks considered in the early days of nanotechnology development.[10–12] Nanotoxicologists have proposed various screening strategies that involve grouping and prioritizing nanomaterials for further testing prior to widespread commercialization.[13–15] Screening approaches have been applied to case studies based on carbon nanomaterials, metal oxides, amorphous silica and pigments.[16,17]

In parallel to this nanosafety work, the nanosynthesis field has advanced rapidly to demonstrate wholly new classes of materials, challenging nanosafety researchers to keep pace. One of those classes is atomically-thin, sheet- or plate-like particles: the so-called "two-dimensional" (2D) materials. The 2D material field has now moved beyond graphene, now including a very large number of new nanosheet materials with chemical and morphological diversity.[18] The number of layered crystals, from which new 2D materials may be created by exfoliation, has been computationally estimated at 6,000,[19] making systematic hazard screening difficult, time consuming and costly. To address this challenge, an early hazard screening framework has been recently proposed for 2D materials.[20] The screening method uses simple biodissolution kinetic studies in reactive media specially chosen for each material to match chemically feasible degradation pathways, either oxidative, reductive, or non-redox. Reactive dissolution and in vitro toxicity tests on the nanosheets and their degradation products allow grouping of materials into four classes: A, potentially biopersistent; B, slowly degradable (>24-48 hours); C, biosoluble with potentially hazardous degradation products; and D, biosoluble with low-hazard degradation products.[20] Performing this classification can accelerate hazard identification and safety assessment by: (i) prioritizing a subset of persistent materials (Class A,B) for more detailed toxicity testing on the specific nanomaterial form in question, (ii) identifying materials that are less likely to pose important health risks (Class D) and (iii) finding a set of materials (Class C) for which the hazard assessment can avoid extensive nanotoxicity testing and

instead use existing data on the *chemical* toxicity of soluble degradation products. The present article focuses on the biodissolution of manganese dioxide (MnO_2) nanosheets as a new case study in the development and validation of the framework.

Manganese dioxide materials are currently used in applications that include cathodes in alkaline and lithium-ion batteries and liquid-phase catalysts.[21–23] In 2010, over 130,000 metric tons of single-use alkaline batteries were estimated to have been shipped to the United States.[24] Substantial research efforts are now focused on substituting particulate MnO_2 with 2D MnO_2 nanostructures to improve performance.[25,26] Recently, MnO_2 nanosheets have been developed as gas-phase catalysts and as electrodes for pseudocapacitors.[27–33] MnO_2 nanosheets also have potential biomedical applications for cellular glutathione (GSH) detection,[34] intracellular microRNA detection,[35] tunable MRI contrast agents[36] and drug delivery platforms.[37]

Manganese is an essential trace metal for all living organisms[38] that is required for antioxidant defense in mitochondria, intermediary metabolism and normal development.[39] In vertebrate animals, uptake of manganese is mainly from the diet and only ~5% is absorbed from the intestine. Manganese homeostasis is tightly regulated in the gastrointestinal tract and excreted by the liver into the bile and by enterocytes into the small intestine.[40,41] Manganese is stored in the liver, kidneys, brain and bone[42] and excess manganese accumulation from occupational or environmental sources can induce toxicity affecting the brain and liver, especially in neonates.[42,43] Inhalation of airborne manganese particles into the lungs can deliver manganese directly into the circulation and particles may translocate to the brain via the olfactory bulb, by-passing the blood-brain barrier and homeostatic mechanisms in the liver and the central nervous system.[44,45] Miners, smelter workers, millers, welders and battery workers are at risk for development of adverse neurobehavioral effects and the clinical syndrome called manganism following inhalation of manganese particles and manganese-containing fumes.[38,46,47]

Manganese is a transition metal with multiple oxidation states, of which Mn^{3+} and Mn^{2+} are most common in biological systems.[46] Mitochondria are the major target of manganese toxicity where it inactivates key enzymes involved in oxidative phosphorylation, metabolism and calcium and iron homeostasis.[42,48] Manganese is redox active and can cause secondary toxicological effects through the generation of excess intracellular reactive oxygen species.[49,50] Manganese oxide particles and nanomaterials may enter aquatic environments through wastewater treatment plant effluents, direct release from products containing engineered nanomaterials (ENMs), run-off from terrestrial sources or through atmospheric releases.[51,52] While the natural level of manganese in freshwater ranges from 0.01-10 mg/L,[53] manganese levels at contaminated sites in the Brazilian Amazon Basin have been measured as high as 264 mg/L.[54] Manganese exists in the aquatic environment in two oxidation states: Mn^{2+} (soluble) and Mn^{4+} (particulate). Interconversion between these two forms can occur in nature due to bacteria-catalyzed oxidation and metal reducing microorganisms.[53] Fish serve as a valuable indicator species for both the detection of contaminated freshwater ecosystems and identifying potential toxicity of pollutants. Tjälve et al.[55] showed that manganese ions can bypass the blood-brain barrier and enter the brains of live fish through the olfactory bulbs. Manganese ions also accumulate in the gills, liver and kidney of fish,

[56,57] resulting in the generation of reactive oxygen species, oxidative damage and impairment of mitochondrial activity.[56,58–60]

Another lesson from the last decade of nanosafety research is the importance of nanomaterial biotransformations.[61] As biological systems respond to nanomaterial exposures, nanomaterials themselves can also "respond" to their exposure to biological environments. This material "response" can take many forms, including degradation, dissolution, surface modification, or chemical reaction with bulk phase change that fundamentally alters the nature of the material toxicant that encounters the target receptor. Understanding material biotransformations can be key to the design of in vitro toxicity tests, if we want them to accurately reproduce the specific toxicant form that is present in the modelled exposure scenario.

In the case of MnO_2 nanosheets, dissolution in environmental or biological systems can release potentially toxic ions including Mn^{2+}, and it may be unclear whether toxicity is associated with the as-produced nanosheet or soluble dissolution products,[18] as described previously for silver nanoparticles.[62–64] The biodissolution of MnO_2 and its classification in the 2D material hazard screening framework[20] presents an interesting case study. MnO_2 is reported to be highly insoluble in water,[65] but capable of reductive dissolution in the presence of electron donors to release Mn^{2+} ions accompanied by material degradation. The timing, location, and biomolecular reaction partners for this MnO_2 reductive dissolution process in unintended exposure scenarios is poorly understood, but is critical for hazard identification and risk assessment and management. The present study characterizes the chemical reaction dynamics and colloidal dynamics of MnO_2 nanosheets in biological media and discusses their implications for environmental risk, human health risks, and in vitro nanotoxicity testing and nanosafety assessment.

2. Results

Self-assembled MnO_2 nanosheets were chemically synthesized for this study and their atomic and geometric structure were characterized (Figure 1). They have lateral dimensions ranging from about 100-300 nm and are approximately equi-axed in plane (having X-Y aspect ratios near unity). Most have thickness from 1-3 nm and are thus a mixture of monolayer and few-layer nanosheets. Some of the nanosheets are flexible, showing spontaneous wrinkling and folding on TEM grids (Figure 1B), and are revealed by X-ray diffraction to be the δ-phase MnO_2 (Figure 1C), a layered phase of interest for new pseudocapacitor electrodes.[66,67] Overall this surfactant templated growth method[32] produces a high-quality, uniform model product material suitable for nanosafety studies. Structural information on the MnO_2 particulate (non-2D) reference material used in this study is found in Figure S2.

Figure 2 shows the dynamic colloidal behavior of MnO_2 nanosheets when introduced into a range of aqueous media. The nanosheets form stable suspensions in nanopure water, but slowly agglomerate in phosphate buffered saline (PBS) or simulated moderately hard water (MOD) over the course of 60 min (Figure 2A). The zeta potential of the 2D MnO_2 in nanopure water is −37 mV, which is generally thought to be sufficient to establish colloidal

stability through electrostatic repulsion.[68] Ionic charge screening[69,70] is the likely cause of the observed agglomeration in the salt-containing MOD and PBS phases, as indicated by zeta potential values that rise to about −20 mV in those media (Figure 2C). The pH dependence of zeta potential is shown in Fig. 2D for both the nanosheets and particles. Both physical forms of MnO_2 show negative surface charge across the entire pH range studied (3 to 10). Full compositions of MOD and PBS are found in Table S1 through S6.

Toxicological screening of engineered nanomaterials is carried out using a variety of target cells in vitro.[5,71,72] Serum is commonly added to media in cell culture studies to provide essential nutrients to the cells although it adds additional complexity for interpreting experimental results. The 2D MnO_2 nanosheets are observed to agglomerate rapidly (<5 min) and settle in serum-free cell culture media, which is consistent with their saline based (~100mM NaCl) formulation. The addition of fetal bovine serum (FBS) to these three cell culture media stabilizes the nanosheet suspensions allowing dynamic light scattering (DLS) screening analysis to show no significant agglomeration over one hour (Figure 2B). While increases in DLS measured hydrodynamic size increases can be interpreted as agglomeration and colloidal instability, decreases in size or loss of signal may be attributed to dissolution. Data in Figure 2 data give no indication of significant dissolution in these media, therefore, direct measurement of soluble manganese (rather than particle size monitoring) is required for accurate characterization of biodissolution (vide infra). Similar results were observed for the reference particulate MnO_2 material (Figure S2).

The results in Figure 3 characterize the chemical dynamics of MnO_2 nanosheets in a set of biological media relevant for safety assessment. Dissolution kinetics were studied by time-resolved measurement of total dissolved Mn by ICP-OES following removal of unreacted solids by ultrafiltration.[73] No significant dissolution of 2D nanosheets occurs in simple aqueous phases (Figure 3A) over 72 hrs. The nanosheets were also stable in Roswell Park Memorial Institute Media (RPMI) and Eagle's Minimum Essential Media (EMEM), but showed a slow, gradual and partial dissolution over 72 hrs in Leibovitz's L15 cell culture medium (Figure 3B). The MnO_2 particle reference sample showed qualitatively similar behavior in both simple and complex media (Figure S4, Figure S5), again showing slow and partial dissolution only in L15 medium. The addition of individual biological antioxidants (cysteine, glutathione (GSH), or ascorbate) to either L15 or to PBS led to rapid (~5 min to 1 hr) and complete dissolution of 2D MnO_2 (Figure 3D). These rapid kinetics indicate that the observed much slower kinetics in L15 cannot be due to the presence of either of these two antioxidants (Figure 3B, 3C). Further, when the oxidized form of the amino acid cysteine (cystine, inactive) was added to L15 medium, no dissolution was observed (Figure 3C), consistent with the expected reductive nature of MnO_2 dissolution.[74]

To explore the slow (72 hr) partial dissolution process in L15 cell culture medium, we conducted amino acid profiling of the cell culture medium before and after acellular exposure to MnO_2 materials under a variety of conditions. Amino acid concentrations were measured after 72 hr exposure, to assess the cumulative effects of media exposure due to slow reaction over the full course of the experiment (Figure 3E). Amino acid concentrations were also measured during short-time exposures (10 min) to assess the relevance of physical adsorption of amino acids onto MnO_2 surfaces, which can deplete solutes in free solution

rapidly due to the absence of an activation energy barrier. Most conditions have a negligible effect on L15 medium composition, but there are important exceptions such as lysine, histidine, and arginine, which show subtle but significant depletions after only 10 min exposure (Figure 3E, Table S8). After 72 hr exposure to the high concentration of MnO_2 nanosheets, tryptophan and tyrosine were depleted much more than the other amino acids. We were particularly interested in concentration differences arising between the 10 min "starting point" and the 72 hr time point (after any physical adsorption had occurred, but before a significant fraction of MnO_2 had chemically reacted). Such a difference would reflect any effects of the gradual MnO_2 dissolution process seen in Figure 3B,C. Statistically significant ($p<0.005$) depletion of tyrosine, tryptophan, and methionine was observed between the 10 min and 72 h timepoints; all for the 2D nanosheet (not reference particle) cases and all at the high materials concentration (1 mg/ml) (Figure S6, Table S9). These three amino acids are among the six most easily oxidized amino acids,[75,76] based on the reduction potentials of their single electron oxidation products at pH 7 (an approximation of physiological conditions).[75] These amino acids are also cited as among the most susceptible to oxidative damage during storage and use.[76] Further, tyrosine, tryptophan and methionine showed the three highest rate constants as electron donors for repair of DNA guanyl radicals[75] among the amino acids profiled here. It is interesting that the unreactive amino acids lysine, histidine and arginine, which all show subtle but significant depletion after 10 min, also possess net positive charge under physiological conditions. Knowing the MnO_2 nanosheets are negatively charged at physiological conditions (Fig. 2C, D), we propose that these amino acids show the most significant amount of physical adsorption on MnO_2 nanosheets, and an important driving force for this physical adsorption is electrostatic attraction. Overall, the patterns observed for 15 amino acids before and after incubation with MnO_2 are consistent with the main dissolution process being slow chemical reduction of MnO_2 through redox reactions involving multiple weak reducing agents in L15 cell culture medium.

Glutathione is a key biological antioxidant[77,78] whose direct interaction with MnO_2 and the resulting dissolution products deserves closer study. Figure 4 shows the time-dependent depletion of glutathione in an acellular assay, in which 1 mM GSH in PBS is mixed with MnO_2 nanosheets, particles, or soluble $MnCl_2$ individually and the unreacted GSH measured with Thiol Fluorescent Probe IV (Millipore). The MnO_2 solids, but not soluble $MnCl_2$ (Mn^{2+} ion), are observed to deplete GSH in a time-dependent manner relative to the untreated control (Figure 4A). Glutathione reductase is an essential enzyme responsible for recycling oxidized glutathione disulfide (GSSG) back to its reduced form (GSH).[79] Following depletion by MnO_2 solids, the GSH can be fully recovered by addition of the enzyme glutathione reductase and its cofactor NADPH, indicating that the GSH oxidation product is the disulfide, GSSG (Figure 4B). Further oxidation beyond the disulfide (e.g. to sulfenic acids) are typically irreversible, further supporting that the recovery is through the conversion of GSSG to reduced GSH.[80,81] It is noteworthy that the extent of GSH depletion in Figure 4 is greater than can be accounted for by direct reaction with MnO_2 as a stoichiometric oxidant at the solids loading used, suggesting some additional contribution from catalysis of the O_2-GSH reaction.[82]

The reductive transformation of MnO_2 nanosheets in biological fluids, and the timing and location of those reactions that degrade the 2D sheets and release Mn^{2+} ion, are expected to affect cellular uptake, biological effects, and toxicity. We chose to study the location and timing of MnO_2 reductive dissolution in an in vitro system using the fish gill cell line, RTgill-W1 cultured in L15 cell culture medium. Fish gills are delicate, highly-vascularized tissues that control respiration, osmoregulation, excretion, and acid-base balance.[83] Gills are an initial target site of exposure to aquatic environmental pollutants[83] and accumulate nanomaterials through their association with mucous proteins on the surface of the gill.[49,84] Carbon nanotubes and a variety of metal oxide nanoparticles induce severe gill irritation, elevated ventilation rates and morphological alterations to the gill tissue.[49,84,85] In addition to increased ventilation rates and thickening of the epithelial tissue along the primary gill filament, exposure to single walled carbon nanotubes induced aggressive behavior amongst rainbow trout (*Oncorhynchus mykiss*) that resulted in fish death. This observation shows that disruption of gill function adversely affects fish and their survival.

Figure 5 shows that both MnO_2 nanosheets and reference particles are found intact and are interacting with cell surface membranes after 3 hr (Figure 5A,C) and 24 hr (Figure 5B,D). TEM imaging of nanosheets (Figure 6A, 6B) and particle (Figure 6C,6D) internalization in fish gill cells confirmed their intracellular localization within vacuoles 24 hr after exposure. It is clear that some MnO_2 nanosheets and particles survive in the L15 cell culture medium for sufficient time to reach the cell surface and initiate uptake.

Rainbow trout gill tissue contains approximately 1.2 – 1.6 μmol GSH/g tissue.[86,87] Similar GSH levels were measured in untreated RTgill-W1 cells (data not shown). For comparison, human lung epithelial cells in vitro contain ~50-150 μmol/g protein.[78] To investigate whether our acellular observations of GSH depletion by MnO_2 nanosheets accurately predict intracellular reactions, we exposed RTgill-W1 cells to MnO_2 nanosheets or particles and measured intracellular GSH levels after 3, 24 or 48 hrs (Figure 6E). We also exposed cells to a Mn^{2+} compound ($MnCl_2$), which is not expected to react with GSH due to its 2+ oxidation state. The pattern of GSH depletion activity in this intracellular assay is the same as in the acellular experiments of Figure 3, (MnO_2 nanosheets > MnO_2 particles > Mn^{2+} ion (inactive), suggesting a similar mechanism, namely direct interaction between MnO_2 solids and intracellular GSH.

Cytotoxicity of the MnO_2 nanosheets was established using a calcein AM stain for live cells and ethidium homodimer 1 stain for dead cells (Figure 7). Exposure to MnO_2 nanosheets induced a significant decrease in cell viability after 72 h, resulting in a LC_{50} of 188 ppm Mn (297 ug/mL) (Figure S7). Cytotoxicity was delayed (no significant cytotoxicity was observed after 48 h exposure) presumably due to the time required for cellular uptake and intracellular dissolution to occur (data not shown). The MnO_2 nanosheets were more cytotoxic than the MnO_2 particles.

3. Discussion

3.1 The MnO_2-biological interface

MnO_2 nanosheets show complex colloidal dynamics and biochemical reactivity that have important implications for environmental health risks and nanosafety testing. First, this work shows that 2D MnO_2 nanosheets and the reference MnO_2 particles form electrostatically stabilized colloidal suspensions over a wide range of pH due to persistent negative charge (Figure 2). Net negative charge in layered manganese oxide materials (the so-called phyllomanganates) such as delta-MnO_2 has been associated with Mn vacancies or Mn3+ lattice substitutions for Mn^{4+}.[93,94]

A distinctive feature of MnO_2 nanomaterials is their biochemical reactivity. They are highly insoluble in water, but have reduction potentials within the range of the cellular redox potential.[18,88] The MnO_2/Mn^{2+} redox couple has a standard electrochemical potential of +1.23 V, which provides a thermodynamic driving force for MnO_2 to directly oxidize a wide variety of biomolecules. During these reactions, MnO_2 in the +IV oxidation state is reduced to the soluble Mn^{2+} +II oxidation state often through the formation of a number of different intermediates.[89] The specific biological targets and the location and timing of these reactions in complex exposure scenarios or during in vitro nanotoxicity testing is poorly understood. Results in Figures 3 and 4 show rapid reaction with ascorbate[89] and with thiol antioxidants cysteine or GSH. The overall reaction with cysteine or GSH has been reported[90–92] to be:

$$2RSH + MnO_2 + 2H^+ = = > Mn^{2+} + RSSR + 2H_2O$$

The reaction of cysteine with 2D or particulate MnO_2 is faster than the same reaction with GSH (Figure 3D, SI4). This is consistent with the rank order of cysteine and GSH oxidation by bulk MnO_2 reported in the literature.[89] The difference in reaction rate has been attributed to increased steric hinderance of the SH group on cysteine when incorporated in the tripeptide GSH.[89] Finally, the chemical behavior of MnO_2 nanosheets (Figures 3–5) is quite similar to that of the MnO_2 particles (Figure 2D,5,6 S3,S4,S5) used as a reference material, except the nanosheet reaction rates are consistently higher. Much of this difference can be explained by the higher specific surface area of nanosheets (400 m^2/g) relative to the particles (32 m^2/g) Figure S1–S2).

A surprising finding of this study is the relative stability of MnO_2 nanosheets in cell culture media (Figure 3). Despite the presence of a large complement of amino acids and micronutrients, high concentrations of reducing sugars (glucose, galactose) or pyruvate as carbon sources, and 3 μM reduced GSH in RPMI cell culture medium (Table S3), and no measurable dissolution of MnO_2 nanosheets is observed in two common commercial media (RPMI, EMEM). A third cell culture medium, L15, induces only a slow, gradual and partial dissolution (~25%) over 72 hrs, which is slow enough that most nanosheets survive their residence time in the extracellular space during in vitro tests and are taken up intact into cells after 24 hrs.

This stability was particularly surprising in light of the known fast reactions with cysteine and glutathione (Figure 3), which are additives in some of the media used. Careful consideration of media compositions (see Table S1–S6) reveals that the amino acid is added in oxidized form (cystine) in some cases, and in other cases air exposure during media handling and storage is likely to oxidize cysteine to the disulfide cystine prior to use.[93] Indeed, addition of fresh cysteine to L15 (Figure 3C) restores the reducing power of the media toward MnO_2 to give similar dissolution kinetics as cysteine in simple PBS (Figure 3D). These data support that cysteine must have been oxidatively deactivated by the time the experiments were conducted to produce the behavior in observed in Figure 3B.[93]

The slow, partial dissolution process in L15 cell culture medium over 72 hrs (Figure 3B) is an interesting feature of this data set. It cannot be due to reaction with ascorbate or glutathione, which are not present in L15. It also cannot be explained through reaction with cysteine, which if present in reduced form at the time of use would react with MnO_2 very rapidly, on a timescale of minutes to one hour (Figure 3C, D) that is not consistent with the slow, gradual process observed in Figure 3B. The slow dissolution of MnO_2 nanosheets in L15 medium is hypothesized to result from the reaction with weaker reductants present in the complex medium, possibly in combination with organic acids that form complexes with the Mn^{2+} to facilitate ion release. In general, media contain a wide variety of oxidizable organic molecules. L15 medium in particular has much higher concentrations of amino acids (sum of 26 mM) than the other media (sum of 5-6 mM) and is the only medium containing pyruvate and the reducing sugar galactose. Analysis of 15 amino acids before and after exposure to MnO_2 suggests that 72 hr exposure to MnO_2 nanosheets causes significant selective depletion of certain amino acids including tyrosine, tryptophan, and methionine, which are known to be three of the most easily oxidized amino acids.[75,76] This depletion occurs between the 10 min and 72 hr time points, consistent with a slow chemical reaction in which MnO_2 is reductively dissolved and multiple reducing agents in the complex L15 medium are oxidized.

The in vitro cellular experiments in Figures 5 and 6 support the predictions of the acellular kinetics studies in Figures 2 and 4. The lack of strong reductants in cell culture media, due to its initial formulation plus age-related deactivation by air oxidation, allow the MnO_2 nanosheets time to reach cells intact, be taken up, and react with intracellular GSH (Figures 5, 6) with associated intracellular release of Mn^{2+} ions that may induce acute toxicity. The patterns in the GSH depletion data in the acellular (Figure 4) and intracellular (Figure 6) data are very similar, suggesting the intracellular depletion is the result of direct interaction between MnO_2 nanosheets and GSH in both scenarios. This interaction involves direct redox reaction that depletes both MnO_2 and GSH, but may also involve catalysis of O_2 oxidation and/or secondary generation of reactive oxygen species, a known factor in Mn-induced toxicity.[39,50,56] Future studies are needed to clarify the biochemical mechanisms that induce toxicity following exposure to 2D MnO_2 nanosheets.

3.2 Implications for Nanosafety

Overall these results provide important insight for evaluating and managing potential environmental and human health risks of MnO_2 nanosheets. First, the results presented here

are sufficient to apply the recently proposed human inhalation hazard screening framework for 2D materials[20] to the case of MnO_2. This framework uses in vitro dissolution studies in reactive simulants to classify 2D materials into one of four categories for rationale hazard assessment and prioritization. While oxidative and hydrolytic degradation routes are common[20,94], MnO_2 is one of the few 2D materials proposed to follow a reductive degradation route,[18] and the first reductive case study in the Gray et al. framework.[20]

Human exposure to MnO_2 nanosheets in the form of aerosols or dry powders is a primary concern in occupational settings. Mathematical modeling of fractional deposition of 2D graphene sheets suggest that thin, plate-like sheets up to 10 μm in lateral dimension will deposit in the tracheobronchial and alveolar regions following inhalation in humans.[95] Inhaled particles deposited in the tracheabronchial regions (conducting airways) of the lungs are removed by mucociliary transport within 24-48 hours, while clearance of particles from the alveoli (air spaces) is prolonged for weeks to months.[96] Clearance of nanoparticles or plate-like graphene sheets from the lungs is even slower[97–99] while spherical nanoparticles (<200 nm in diameter) are more readily translocated across the alveolar epithelial cell barrier into the systemic circulation.[100] Slower uptake and clearance of 2D MnO_2 nanosheets from the lungs would prolong their interaction with extracellular lung lining fluid, which contains approximately 0.5 mM GSH secreted from lung epithelial cells.[77,101] Our results in an acellular assay show rapid GSH-nanosheet reaction times (~1 hr) and it is likely that significant dissolution of MnO_2 nanosheets in the extracellular lung lining fluid would occur more rapidly than slower uptake of intact 2D nanosheets by macrophages or lung epithelial cells. Previous studies using 2D graphene microsheets (0.5-25 μm in lateral dimension) showed uptake by macrophages and human lung epithelial cells in vitro after 5 and 24 hrs, respectively.[102] Therefore, in the context of this 2D material hazard screening framework for human inhalation exposure,[20] MnO_2 nanosheets would be classified as “biosoluble” leading to further consideration of toxicity of the soluble degradation product, manganese ions. Inhalation of manganese oxide particles under occupational conditions delivers manganese ions to the systemic circulation and the brain leading to manganism.[38,45,46] Therefore, inhalation of MnO_2 nanosheets followed by reductive dissolution releasing manganese ions in the lungs places this material in Class C: “biosoluble with potentially hazardous dissolution products”

This argument is applicable for the 2D MnO_2 nanosheets synthesized in this study that are ~300-500 nm in lateral dimension and would be predicted to deposit mostly in the tracheobronchial or alveolar regions in the human respiratory tract.[96] However, for smaller nanosheets, as predicted for 2D graphene nanosheets (~1-10 nm in lateral dimension), the majority of nanoparticles would be predicted to deposit by diffusion in the upper respiratory tract or nasopharyngeal region.[96,103] Elder et al.[44] generated spherical manganese oxide nanoparticles (primary particle diameter 3-8 nm; agglomerates ~30 nm airborne median diameter of agglomerates in the aerosol) and demonstrated deposition in the olfactory mucosa and translocation of solid manganese oxide nanoparticles to the olfactory bulb and the brain following inhalation in rats. These nanoparticles were poorly soluble in physiological saline at neutral pH and additional studies suggested that soluble Mn shows limited uptake via the olfactory route in the rat (Elder et al.)[44] In humans, GSH content of the nasal fluid is below the limit of detection (0.5 μM)[104] so it is unlikely that small MnO_2

particles or nanosheets would undergo reductive dissolution in the upper respiratory tract. However, it is unknown whether intact 2D MnO_2 nanosheets with lateral dimensions in the range of 1-10 nm would be translocated into the brain via the olfactory route in humans because surface chemistry and shape modify deposition and translocation of nanoparticles in the upper and lower respiratory tract.[103] Additional experimental data and pharmacokinetic modeling are required for dosimetry-based risk assessment of inhaled MnO_2 nanosheets in humans.[38,105,106]

Chemical and colloidal dynamics of MnO_2 will also affect behavior and risk in the natural environment. MnO_2 nanosheets are shown here to be indefinitely stable in simple aqueous media, but sensitive to interactions with diverse electron donors. Natural organic matter[107,108] has been reported to reductively transform Mn oxides releasing soluble Mn^{2+} ions.[49,84,109] Mn^{2+} accumulates in the brain, gills, liver and kidney of fish, inhibiting mitochondrial activity and inducing oxidative damage.[56–60] Alternatively, Mn^{2+} could be converted back to particulate Mn^{4+} by bacterially-catalyzed oxidation.[53] The constant perfusion of water makes fish gills a target site for environmental toxicants and nanomaterials. The data presented in this paper suggest MnO_2 particles taken up by gill cells would oxidize GSH intracellularly, dissolving during the reaction to Mn^{2+} ions and potentially generating secondary reactive oxygen species, leading to mitochondrial damage and oxidative stress. VanWinkle et al.[110] observed similar uptake of spherical manganese oxide particles (40 nm in diameter) by alveolar epithelial cells in vitro resulting in uptake into lysosomes and generation of H_2O_2. Therefore, fish gill epithelial cells may be a useful model for investigation of biological and chemical interactions of manganese oxide particles and nanosheets with mammalian lung epithelial cells.

Finally, these results have implications for the design of in vitro nanotoxicity testing platforms and protocols. Despite publication of over 10,000 peer-reviewed papers on environmental and health impacts of nanomaterials since 2001,[1] concerns remain about technical caveats and artifacts in nanotoxicology assays that limit extrapolation to in vivo endpoints.[5,6,111] Very little attention has been paid to the design of toxicity tests for materials sensitive to reductive transformations, making MnO_2 nanosheets an important new case study. We observed 2D MnO_2 nanosheets to be stable in cell culture media and thus to enter cells intact where they react with intracellular GSH to degrade and deliver Mn^{2+} ions. In general, however, we expect this behavior to depend on the redox state of the cell culture medium used, which in turn is determined by its composition and handling/storage history. “Fresh” media with cysteine (reduced form) or GSH may show the opposite behavior, in which MnO_2 nanosheets degrade in the extracellular space, and liberate Mn^{2+} ions, which likely become the primary toxicant in the test system. These results show that care is needed to design and interpret in vitro toxicity tests that are meaningful for various exposure scenarios to MnO_2 materials depending on the anticipated route of exposure and potential target cells. We suggest that in vitro tests consider the effect of the composition and redox state of the media and extracellular nanomaterial dissolution kinetics in order to understand the contribution of extracellular dissolution to toxicological endpoints. It is also important to include soluble Mn controls, since the Mn^{2+} ion is highly likely to be present in biological systems, despite the standard classification of MnO_2 materials as highly insoluble.

4. Conclusions

Manganese dioxide nanosheets show novel and important chemical and colloidal dynamics in fluid media relevant to environmental and human exposures. The nanosheets exhibit a dominant negative charge over the full relevant pH range and form electrostatically stabilized colloids in low-salt aqueous environments. MnO_2 nanosheets are salt-destabilized in hard water and small-molecule biological buffers, but can be sterically re-stabilized by addition of serum. The MnO_2 solid phase persists indefinitely in simple aqueous media, and has the potential to reach aquatic receptors as intact nanosheets. The nanosheets react rapidly, however, with biological antioxidants and slowly with other molecules in complex biological media. Overall these chemical and colloidal behaviors are similar to those shown by particulate MnO_2, used as a non-2D reference material, but with faster chemical kinetics for the nanosheets (first order GSH rate constant 0.44 L/mol-s) vs. particles (0.036 L/mol-s), consistent with higher nanosheet specific surface area and quantitatively similar to the area ratio (400 vs. 32 m^2/g) The short time scales of reductive dissolution by glutathione allow categorization of MnO_2 nanosheets as a Class C material for inhalation hazard [20] – biosoluble in lung lining fluids, with potentially hazardous degradation products (Mn^{2+}). This finding may allow risk assessment of MnO_2 nanosheets to move forward based on existing data for the well-known chemical toxicant, Mn^{2+} without more extensive nanotoxicity testing on specific 2D formulations.

During in vitro testing, MnO_2 nanosheets are sufficiently stable in three cell culture media to reach cell surfaces, become internalized, and react directly to deplete intracellular GSH. In contrast, media containing fresh thiol antioxidants in the reduced form rapidly degrade MnO_2 nanosheets at time scales shorter than those for cell uptake. Care must be taken in the design of in vitro toxicity tests, including consideration of media composition and air exposure during storage and aging, to understand the form of the toxicant (nanosheets vs. Mn^{2+} ions) encountered by the target cells.

5 Experimental Section

Manganese oxide materials:

MnO_2 nanosheets were synthesized using an adaptation of the aqueous-phase bottom-up method described by Liu et al.[32] Briefly, nanosheets assemble by reduction of $KMnO_4$ precursor [112–114] and nucleation on sheet-like dodecanol templates derived in situ from hydrolysis of the surfactant sodium dodecyl sulfate (SDS). A large round bottom flask containing approximately 2.2L of deionized water (18.2 MΩ, milli-Q pore) was heated to 95°C, using hollow water balls to maintain water bath temperature and volume. SDS and H_2SO_4 solutions were added to the flask resulting in concentrations of 0.23M for each compound. After 15 minutes, a $KMnO_4$ solution was added to the mixture slowly (to maintain reaction temperature), resulting in an overall concentration of 17.9 mg/L and turning the reaction a deep purple. This mixture was maintained at 95°C for 60 minutes, changing the solution from deep purple to a light and dark brown mix where some large MnO_2 aggregates were visible. The reaction was quenched by lightly filtering the obtained MnO_2 product using vacuum filtration through a 0.22 μm pore-size sterile disposable vacuum filter (Corning, Corning, New York, USA). The product was washed six times

alternating between 100% ethanol and nanopure water, using approximately 1L of wash liquid each rinse. The MnO_2 product was never allowed to dry during washing, and the filtrate was clear indicating all the MnO_2 was collected on the filter. The washed MnO_2 product was transferred to a sterile 50 ml centrifuge tube (Corning, Corning, New York, USA). MnO_2 particles in powder form (Sigma Aldrich 310700) were used as-received as a non-sheet-like reference material. Both the nanosheets and particles were stored as aqueous suspensions in 18MΩ water at 4°C for the duration of the project.

Material Characterization:

The MnO_2 materials were characterized using scanning electron microscopy (SEM, Zeiss LEO 1530), transmission electron microscopy (TEM, JEOL 2500), X-ray diffraction (XRD, Bruker Eco Advance), nanosheets are characterized by AFM (Asylum MFP-3D Origin) operating in alternating contact mode. and dynamic light scattering (DLS) for electrophoretic mobility/zeta potential (Malvern Zetasizer). Total Mn concentrations in suspension were determined by inductively coupled plasma optical emission spectrometry (ICP-OES, Thermo Scientific iCAPtm 7400) after diluting the MnO_2 stock suspension in 2% HNO_3 and adding 100 μL of H_2O_2 as a reductant to convert all MnO_2 to Mn^{2+}. A Quantachrome Autosorb-1 instrument was used to obtain a MnO_2 power N_2 isotherm at 77K from which the surface area based on the Brunauer–Emmett–Teller (BET) theory and pore size distributions (PSD) based on non- local density functional theory (NLDFT) slit pore model[115] were calculated. The BET surface area was calculated from N_2 adsorption isotherm relative pressures ranging from 0.05 to 0.30, when nearly perfect linear BET correlation ($R^2 = 0.9999$) was observed. 2D MnO_2 surface area was determined through adsorption of methylene blue (MB, Aldrich Chemical Company, Inc.) dye following Langmuir adsorption. MB adsorption was tested in glass vials at 0.15 mg/ml using 2D MnO_2 while MB concentrations varied from 10, 20, 30, 40 and 50 mg/L. All waterMnO_2 suspensions were sonicated for one hour prior to preparing isotherms. All experimental reactors were shaken in the dark at 220 rpm for three hours at 22 °C after which suspensions were filtered using 0.2μm filters to remove remaining MnO_2 solids. The residual MB concentrations were determined using a JASCO V-730 UV-Visible spectrophotometer at 664 nm. Experiments were conducted at pH>4 to prevent oxidative MB degradation that occurs at pH<4. Further, MB degradation shifts peak absorbance to 600 nm, while peak maxima were observed at 664 nm here, ensuring no MB degradation occurred during adsorption experiments.

Biodissolution kinetics and colloidal dynamics:

Time-resolved dissolution measurements were made on MnO_2 nanosheet and particles exposed to a set of common aqueous fluid phases and biologically-relevant media: nanopure water (NP H_2O), EPA standard moderate-hard water (EPA Mod), phosphate buffered saline (PBS), Roswell Park Memorial Institute cell culture medium (RPMI), Leibovitz's L15 cell culture medium (L15), and Eagle's Minimum Essential Medium (EMEM). The complete formulations are listed in Tables S3 to S7. During all experiments, the media were never diluted below 90% of their original compositions. Biodissolution was monitored by time-resolved measurement of total soluble Mn (presumed to be Mn^{2+}) following removal of nanosheets or particles by ultrafiltration. These studies were carried out in 50 mL centrifuge

tube reactors (Corning, Corning, New York, USA) with 8.69 mg/L starting MnO_2 concentration in a rotational mixer (Fisher Scientific, Waltham, MA), from which sacrificial subsamples were taken at each time point for analysis. Solids were removed using a 20 nm Anatop filter (Milipore), and total dissolved Mn concentration in the filtrate was determined by Inductively Coupled Plasma Optical Emission Spectroscopy (ICP-OES) using a Thermo Scientific iCAP^{tm} 7400 ICP-OES. Three experimental replicates were used to quantify variability. Experiments involving biological reductants were designed to use a 5:1 molar equivalence ratio between reductant and MnO_2 (requiring two electrons per mole from Mn(IV) to Mn(II) in order to ensure that the reductant was not the limiting reagent in the experiment with the exception of ascorbic acid, which used a 10:1 ratio

Dynamic Light Scattering (Malvern Zetasizer *Nano ZS* (Worcestershire, United Kingdom) operating at 90° scattering angle was used to make time-resolved measurements of particle or agglomerate hydrodynamic diameter. For DLS analysis, 2D MnO_2 was purified using centrifugation, removing heavier fractions until a more uniform distribution was obtained. The resulting solution was tested at 1.1 mg/L and was required to meet data quality objectives Decreases in the hydrodynamic diameter imply dissolution of the material, while increases provide information on the rates and extents of nanosheet or particle agglomeration.[116] The reported sizes are a sphere-equivalent hydrodynamic diameters, and for the high-aspect-ratio nanosheet materials are best used as qualitative comparative values. Zeta potential measurements were taken using a Malvern Zetasizer *Nano ZS* (Worcestershire, United Kingdom) to determine the electrostatic stability of the nanosheet and particle MnO_2 across various relevant media (NP H_2O, EPA Mod, PBS, RPMI, L15, and EMEM), and pH buffers. No purification steps were taken prior to zeta potential measurement. Additional zeta potential measurements were taken using buffers ranging from pH 3 to 10. The buffers used were sourced from Fisher Scientific: pH 3 and 4 buffers were potassium phthalate based; pH 6 and 8 buffers were phosphate based while pH 10 buffer was composed of EDTA and carbonate. MnO_2 was added to 5mL aliquots of media/buffer to achieve a 50mg/L MnO_2 concentration. Samples were vortexed for 60 seconds to ensure homogeneity. 1mL of the sample was then transferred to a Malvern Folded Capillary Zeta Cell (DTS1070) and loaded into the Zetasizer. Each sample consisted of a triplicate measurement for precision

In Vitro Cellular Studies:

The in vitro biological model chosen for this study was the well-characterized fish gill cell line, RTgill-W1 (ATCC CRL-2523), derived from rainbow trout (*Oncorhynchus mykiss*). Fish and in vitro fish cell lines have been utilized as models in toxicological testing of heavy metals and nanomaterials for over two decades.[31,117] Well-characterized rainbow trout cell lines derived from rainbow trout gill (RTgill – W1) are differentiated in monolayer cultures, express xenobiotic metabolizing enzymes and membrane transporters and have been validated for aquatic toxicity testing.[118–121] Fish gill epithelial cells have similar physiological functions as mammalian lung epithelial cells that are essential for gas exchange, ion transport and mucous secretion to provide a barrier against particulates and microorganisms.[83,85] This rainbow trout gill cell line has morphological features similar to mammalian lung epithelial cells including abundant mitochondria that are potential targets

for manganese toxicity.[46] RTgill-W1 cells were cultured in L15 medium supplemented with 10% fetal bovine serum and 1% penicillin/streptomycin, maintained at 19°C and sub-cultured weekly. 2D MnO_2 nanosheets and MnO_2 particles suspended in sterile water were sonicated in a bath sonicator for 1 hr. MnO_2 materials were then diluted to 224 ug/mL in serum-free L15 medium and sonicated for 15 min before final concentrations were prepared in serum-free L15 medium. Manganese (II) chloride tetrahydrate (Sigma Aldrich M3634) was dissolved in sterile water at 500mM before dilutions were prepared in serum-free L15 medium at equivalent ionic Mn concentrations as in fully dissolved MnO_2 (Table S7).

Amino Acid Depletion Analysis:

The depletion of 15 amino acids from L15 culture medium after incubation with 2D and particulate MnO_2 was performed as described in Creighton et al.[122] with minor alterations. Briefly, MnO_2 materials suspended in ultra-pure water were sonicated for 1 h and added to serum-free L15 medium (Gibco) at doses ranging from 0.05 to 1 mg/mL. Samples were vortexed and rocked on a lab rocking platform for 10 mins or 72 h. To control for different dilution factors between MnO_2 doses, untreated controls were diluted by the same dilution factor as each dose of MnO_2 materials. MnO_2 materials were separated from cell culture media by centrifugal ultrafiltration using Amicon Ultra-15 filter tubes and centrifuging for 30 min at 4000 g. Samples were then frozen at −20°C and amino acid depletion analysis was conducted by Life Technologies Corporation. Amino acid concentrations were determined by high performance liquid chromatography with UV detection. Results were expressed as the mean ± standard deviation of 3 independent experiments. Statistical analyses were performed as two-way ANOVAs followed by Sidak's multiple comparisons tests using GraphPad Prism 8.0.2 software.

Cellular and Acellular Glutathione Assays:

To characterize the interactions of manganese compounds with glutathione, the abundant intracellular reducing agent, MnO_2 nanosheets, MnO_2 particles or soluble $MnCl_2$ (5.5 ppm Mn ions 8.7 μg/mL MnO_2) were individually mixed with 1mM reduced glutathione (GSH) in PBS (pH 7.4) with continuous agitation for 3, 24 or 48 h. After each timepoint, reduced glutathione was measured by fluorescence using a Thiol Fluorescent Probe IV (Millipore) that acts as a thiol/sulfhydryl detector. Fluorescent values were read with a SpectraMax2 (Molecular Devices) and converted to GSH concentrations based on a GSH standard calibration curve using the SpectraMax2 SoftMax Pro version 5.4.1 software (Molecular Devices). The enzyme glutathione reductase and its cofactor NADPH were added after 48 h exposure to MnO_2 particles and nanosheets at a final concentration of 0.5 U/mL and 4.5 mM, respectively and mixed with continuous agitation for 15 mins at 25°C in order to recover the original concentration of reduced GSH.

Intracellular GSH levels were determined after exposure of fish gill cells to MnO_2 nanosheets, MnO_2 particles or soluble $MnCl_2$ (10 ppm Mn ions) for 3, 24 or 48 h. At the end of each exposure time, cells were washed with PBS (pH 7.4) and incubated on ice in passive lysis buffer (Promega Corporation) for 10 min with or without NEM (N-ethylmaleimide). Cell lysates were collected, incubated on ice for another 15 min and centrifuged at 15,000 rpm for 10 min before the GSH/GSSG-Glo assay (Promega Corporation) was performed

according to manufacturer's instructions. Protein content of the cell lysates was quantified using the Pierce BCA Protein Assay kit (Thermo Scientific). GSH was normalized against protein concentration (nmol GSH/mg protein) and presented as relative to control. For both acellular and cellular GSH experiments, results were expressed as the mean ±standard deviation of 3 independent experiments. Statistical analysis was performed as a two-way ANOVA followed by Sidak's multiple comparisons test using GraphPad Prism 8.0.2 software.

Electron Microscopy:

Scanning electron microscopy was used to observe the interaction of MnO_2 nanosheets and particles with the cellular membrane. Briefly, fish gill cells were seeded on Thermanox Plastic coverslips (13mm) and exposed to MnO_2 nanosheets or particles (5.5 ppm Mn ions) for 3 or 24 h. At harvest, samples were washed 3x with PBS and fixed in cold 2% glutaraldehyde in 0.1 mol/L sodium cacodylate buffer (pH 7.2) containing 0.1 mol/L sucrose. Samples were rinsed 3x with cacodylate buffer (0.1M, pH 7.2) and post-fixed in buffered osmium tetroxide (0.5%) in 0.1 M sodium cacodylate buffer for 30 min. Samples were then rinsed in distilled water and immersed in 1% thiocarbohydrazide, followed by 1% osmium tetroxide before being dehydrated in graded ethanols. Finally, samples were submerged in a mix of 100% ethanol and hexamethyldisilazane (1:1) before being air dried and on a Thermo Apreo VS SEM.

Transmission electron microscopy was used to visualize internalized MnO_2 nanosheets and particles. Briefly, fish gill cells were seeded in 6 well plates and exposed to MnO_2 nanosheets or particles (5.5 ppm Mn ions) for 24 or 48 h. At harvest, samples were washed 3x with PBS and fixed in cold 2.5% glutaraldehyde, 2% paraformaldehyde and 2 mM calcium chloride in 0.15 M sodium cacodylate buffer (pH 7.3) for 2 h. Samples were collected and stored at 4°C until being post fixed with 2% osmium tetroxide/potassium ferrocyanide mixture, 1% thiocarbohydrazide, then 2% osmium tetroxide with appropriate rinses between staining steps. Specimens were then stained with 1% uranyl acetate overnight, followed by Walton's lead aspartate (pH 5.5) at 60°C for 30 min. Finally, samples were dehydrated in graded ethanols, infiltrated with Araldite Embed 812 embedding medium (Electron Microscopy Science) and cured at 60°C for subsequent sectioning. Micrographs were obtained on a Philips 410 Transmission Electron Microscope at 60 kV.

Cytotoxicity:

Cytotoxicity was determined after exposure of fish gill cells to MnO_2 nanosheets, or MnO_2 particles (5–100 ppm Mn ions) for 24, 48 or 72 hr. At the end of each exposure time, cells were washed with PBS (pH 7.4) before being stained with a final concentration of 2uM calcein AM and 4 μM ethidium homodimer one in phenol free L15. After 10 min incubation, cells were imaged with a 10x air objective on an Olympus confocal spinning disk microscope. Live (green fluorescence) and dead (red fluorescence) cells were quantified in Cell Profiler and results were expressed as the mean ± standard error of 3 independent experiments. Statistical analysis was performed as a two-way ANOVA followed by Sidak's multiple comparisons test using GraphPad Prism 8.0.2 software. LC_{50} for MnO_2 nanosheets was calculated in Microsoft excel using Finney's Probit analysis.

Supplementary Material

Refer to Web version on PubMed Central for supplementary material.

Acknowledgements

The authors acknowledge financial support from National Institute of Environmental Health Sciences (NIEHS) Superfund Research Program P42 ES013660 and the NIEHS Training Program in Environmental Pathology T32 (ES00727225). Technical assistance from Dr. Indrek Külaots in nitrogen vapor adsorption measurements and technical assistance by Zachary Saleeba in 2D MnO_2 surface area measurements using methylene blue adsorption is gratefully acknowledged.

References

[1]. Krug HF, Angew. Chem. Int. Ed. 2014, n/a.

[2]. Singh AV, Laux P, Luch A, Sudrik C, Wiehr S, Wild A-M, Santomauro G, Bill J, Sitti M, Toxicol. Mech. Methods 2019, 29, 378. [PubMed: 30636497]

[3]. Holden PA, Gardea-Torresdey JL, Klaessig F, Turco RF, Mortimer M, Hund-Rinke K, Cohen Hubal EA, Avery D, Barceló D, Behra R, Cohen Y, Deydier-Stephan L, Ferguson PL, Fernandes TF, Herr Harthorn B, Henderson WM, Hoke RA, Hristozov D, Johnston JM, Kane AB, Kapustka L, Keller AA, Lenihan HS, Lovell W, Murphy CJ, Nisbet RM, Petersen EJ, Salinas ER, Scheringer M, Sharma M, Speed DE, Sultan Y, Westerhoff P, White JC, Wiesner MR, Wong EM, Xing B, Steele Horan M, Godwin HA, Nel AE, Environ. Sci. Technol. 2016, 50, 6124. [PubMed: 27177237]

[4]. Crawford SE, Hartung T, Hollert H, Mathes B, van Ravenzwaay B, Steger-Hartmann T, Studer C, Krug HF, Environ. Sci. Eur. 2017, 29, 16. [PubMed: 28435767]

[5]. Stone V, Johnston H, Schins RPF, Crit. Rev. Toxicol. 2009, 39, 613. [PubMed: 19650720]

[6]. Joris F, Manshian BB, Peynshaert K, De Smedt SC, Braeckmans K, Soenen SJ, Chem. Soc. Rev. 2013, 42, 8339. [PubMed: 23877583]

[7]. Lead JR, Batley GE, Alvarez PJJ, Croteau M-N, Handy RD, McLaughlin MJ, Judy JD, Schirmer K, Environ. Toxicol. Chem. 2018, 37, 2029. [PubMed: 29633323]

[8]. Maynard AD, Aitken RJ, Butz T, Colvin V, Donaldson K, Oberdörster G, Philbert MA, Ryan J, Seaton A, Stone V, Tinkle SS, Tran L, Walker NJ, Warheit DB, Nature 2006, 444, 267. [PubMed: 17108940]

[9]. Schulte PA, Geraci CL, Murashov V, Kuempel ED, Zumwalde RD, Castranova V, Hoover MD, Hodson L, Martinez KF, Nanoparticle Res J. 2014, 16, 2153.

[10]. Colvin VL, Nat. Biotechnol. 2003, 21, 1166. [PubMed: 14520401]

[11]. Oberdörster G, Oberdörster E, Oberdörster J, Environ. Health Perspect. 2005, 113, 823. [PubMed: 16002369]

[12]. Nel A, Xia T, Mädler L, Li N, Science 2006, 311, 622. [PubMed: 16456071]

[13]. Nel A, Xia T, Meng H, Wang X, Lin S, Ji Z, Zhang H, Acc. Chem. Res. 2013, 46, 607. [PubMed: 22676423]

[14]. Arts JHE, Hadi M, Keene AM, Kreiling R, Lyon D, Maier M, Michel K, Petry T, Sauer UG, Warheit D, Wiench K, Landsiedel R, Regul. Toxicol. Pharmacol. 2014, 70, 492. [PubMed: 25108058]

[15]. Godwin H, Nameth C, Avery D, Bergeson LL, Bernard D, Beryt E, Boyes W, Brown S, Clippinger AJ, Cohen Y, Doa M, Hendren CO, Holden P, Houck K, Kane AB, Klaessig F, Kodas T, Landsiedel R, Lynch I, Malloy T, Miller MB, Muller J, Oberdorster G, Petersen EJ, Pleus RC, Sayre P, Stone V, Sullivan KM, Tentschert J, Wallis P, Nel AE, ACS Nano 2015, 9, 3409. [PubMed: 25791861]

[16]. Arts JHE, Irfan M-A, Keene AM, Kreiling R, Lyon D, Maier M, Michel K, Neubauer N, Petry T, Sauer UG, Warheit D, Wiench K, Wohlleben W, Landsiedel R, Regul. Toxicol. Pharmacol. 2016, 76, 234. [PubMed: 26687418]

[17]. Wohlleben W, Hellack B, Nickel C, Herrchen M, Hund-Rinke K, Kettler K, Riebeling C, Haase A, Funk B, Kühnel D, Göhler D, Stintz M, Schumacher C, Wiemann M, Keller J, Landsiedel R, Broßell D, Pitzko S, Kuhlbusch TAJ, Nanoscale 2019, 11, 17637. [PubMed: 31539006]

[18]. Wang Z, Zhu W, Qiu Y, Yi X, von dem Bussche A, Kane A, Gao H, Koski K, Hurt R, Chem Soc Rev 2016, 45, 1750. [PubMed: 26923057]

[19]. Mounet N, Gibertini M, Schwaller P, Campi D, Merkys A, Marrazzo A, Sohier T, Castelli IE, Cepellotti A, Pizzi G, Marzari N, Nat. Nanotechnol. 2018, 13, 246. [PubMed: 29410499]

[20]. Gray EP, Browning CL, Wang M, Gion KD, Chao EY, Koski KJ, Kane AB, Hurt RH, Environ. Sci. Nano 2018, 5, 2545. [PubMed: 31548890]

[21]. Zhang H, ACS Nano 2015, 9, 9451. [PubMed: 26407037]

[22]. Andreozzi R, Insola A, Caprio V, Marotta R, Tufano V, Appl. Catal. Gen. 1996, 138, 75.

[23]. Hasan MA, Zaki MI, Pasupulety L, Kumari K, Appl. Catal. Gen. 1999, 181, 171.

[24]. Cheng F, Zhao J, Song W, Li C, Ma H, Chen J, Shen P, Inorg. Chem. 2006, 45, 2038. [PubMed: 16499364]

[25]. Desilvestro J, J. Electrochem. Soc. 1990, 137, 5C.

[26]. Julien Christian, Mauger Alain, Nanomaterials 2017, 7, 396.

[27]. Kang M, Park ED, Kim JM, Yie JE, Appl. Catal. Gen. 2007, 327, 261.

[28]. Kim SC, Shim WG, Appl. Catal. B Environ. 2010, 98, 180.

[29]. Jiao F, Frei H, Energy Environ. Sci. 2010, 3, 1018.

[30]. Zhu W, Dong Z, Fu T, Liu J, Chen Q, Li Y, Zhu R, Xu L, Liu Z, Adv. Funct. Mater. 2016, 26, 5490.

[31]. Shin J, Anisur RM, Ko MK, Im GH, Lee JH, Lee IS, Angew. Chem. Int. Ed. 2009, 48, 321.

[32]. Liu Z, Xu K, Sun H, Yin S, Small 2015, 11, 2182. [PubMed: 25565035]

[33]. Horvath A, Masanet E, Single-Use Alkaline Battery Case Study: The Potential Impacts of Extended Producer Responsibility (EPR) in California on Global Greenhouse Gas (GHG) Emissions, California Department Of Resources Recycling And Recovery, 2012.

[34]. Yuan D, Ding L, Sun Z, Li X, Sci. Rep. 2018, 8, 1747. [PubMed: 29379132]

[35]. Li S, Xu L, Sun M, Wu X, Liu L, Kuang H, Xu C, Adv. Mater. Deerfield Beach Fla 2017, 29, DOI 10.1002/adma.201606086.

[36]. Bañobre-López M, García-Hevia L, Cerqueira MF, Rivadulla F, Gallo J, Chem. - Eur. J. 2018, 24, 1221.

[37]. Hao Y, Wang L, Zhang B, Zhao H, Niu M, Hu Y, Zheng C, Zhang H, Chang J, Zhang Z, Zhang Y, Nanotechnology 2016, 27, 025101. [PubMed: 26629735]

[38]. Santamaria AB, Sulsky SI, J. Toxicol. Environ. Health A 2010, 73, 128. [PubMed: 20077284]

[39]. Smith MR, Fernandes J, Go Y-M, Jones DP, Biochem. Biophys. Res. Commun. 2017, 482, 388. [PubMed: 28212723]

[40]. Roth JA, Biol. Res. 2006, 39, DOI 10.4067/S0716-97602006000100006. [PubMed: 16629163]

[41]. Mercadante CJ, Prajapati M, Conboy HL, Dash ME, Herrera C, Pettiglio MA, Cintron-Rivera L, Salesky MA, Rao DB, Bartnikas TB, J. Clin. Invest. 2019, 129, 5442. [PubMed: 31527311]

[42]. Chen P, Front. Biosci. 2018, 23, 1655.

[43]. Dorman DC, Struve MF, Vitarella D, Byerly FL, Goetz J, Miller R, J. Appl. Toxicol. JAT 2000, 20, 179. [PubMed: 10797470]

[44]. Elder A, Gelein R, Silva V, Feikert T, Opanashuk L, Carter J, Potter R, Maynard A, Ito Y, Finkelstein J, Oberdörster G, Environ. Health Perspect. 2006, 114, 1172. [PubMed: 16882521]

[45]. Chen P, Chakraborty S, Mukhopadhyay S, Lee E, Paoliello MMB, Bowman AB, Aschner M, J. Neurochem. 2015, 134, 601. [PubMed: 25982296]

[46]. Michalke B, Halbach S, Nischwitz V, J. Environ. Monit. JEM 2007, 9, 650. [PubMed: 17607384]

[47]. Santamaria AB, Cushing CA, Antonini JM, Finley BL, Mowat FS, J. Toxicol. Environ. Health Part B 2007, 10, 417.

[48]. Roth JA, Garrick MD, Biochem. Pharmacol. 2003, 66, 1. [PubMed: 12818360]

[49]. Smith CJ, Shaw BJ, Handy RD, Aquat. Toxicol. Amst. Neth. 2007, 82, 94.

[50]. Kaur G, Kumar V, Arora A, Tomar A, Ashish R Sur D. Dutta, Sci. Rep 2017, 7, 11645. [PubMed: 28928443]

[51]. Sun TY, Gottschalk F, Hungerbühler K, Nowack B, Environ. Pollut. 2014, 185, 69. [PubMed: 24220022]

[52]. Vale G, Mehennaoui K, Cambier S, Libralato G, Jomini S, Domingos RF, Aquat. Toxicol. 2016, 170, 162. [PubMed: 26655660]

[53]. Pinsino A, Matranga V, Carmela M, in Environ. Contam. (Ed: Srivastava J), InTech, 2012.

[54]. Baldisserotto B, Garcia LO, Benaduce AP, Duarte RM, Nascimento TL, Gomes LC, Chippari Gomes AR, Val AL, Arch. Environ. Contam. Toxicol. 2012, 62, 78. [PubMed: 21503699]

[55]. Tjälve H, Mejàre C, Borg-Neczak K, Pharmacol. Toxicol. 1995, 77, 23. [PubMed: 8532608]

[56]. Dolci GS, Dias VT, Roversi K, Roversi Kr., Pase CS, Segat HJ, Teixeira AM, Benvegnú DM, Trevizol F, Barcelos RCS, Riffel APK, Nunes MAG, Dressler VL, Flores EMM, Baldisserotto B, Bürger ME, Ecotoxicol. Environ. Saf. 2013, 91, 103. [PubMed: 23433555]

[57]. Gabriel D, Riffel APK, Finamor IA, Saccol EMH, Ourique GM, Goulart LO, Kochhann D, Cunha MA, Garcia LO, Pavanato MA, Val AL, Baldisserotto B, Llesuy SF, Arch. Environ. Contam. Toxicol. 2013, 64, 659. [PubMed: 23440445]

[58]. Crawford S, Davis K, Saddler C, Joseph J, Catapane EJ, Carroll MA, In Vivo 2011, 33, 7. [PubMed: 21977482]

[59]. Vieira MC, Torronteras R, Córdoba F, Canalejo A, Ecotoxicol. Environ. Saf. 2012, 78, 212. [PubMed: 22154142]

[60]. Dolci GS, Vey LT, Schuster AJ, Roversi K, Roversi K, Dias VT, Pase CS, Barcelos RCS, Antoniazzi CTD, Golombieski JI, Glanzner WG, Anezi Junior PA, Gonçalves PBD, Nunes M. a. G., Dressler VL, Baldisserotto B, Burger ME, Aquat. Toxicol. Amst. Neth. 2014, 157, 175.

[61]. Zhu M, Nie G, Meng H, Xia T, Nel A, Zhao Y, Acc. Chem. Res. 2013, 46, 622. [PubMed: 22891796]

[62]. Yue Y, Behra R, Sigg L, Fernández Freire P, Pillai S, Schirmer K, Nanotoxicology 2015, 9, 54. [PubMed: 24621324]

[63]. Xiu Z, Zhang Q, Puppala HL, Colvin VL, Alvarez PJJ, Nano Lett. 2012, 12, 4271. [PubMed: 22765771]

[64]. Liu JY, Wang ZY, Liu FD, Kane AB, Hurt RH, Acs Nano 2012, 6, 9887. [PubMed: 23046098]

[65]. Howe PD, Malcolm HM, Dobson S, Manganese and Its Compounds: Environmental Aspects, World Health Organization, Geneva, 2004.

[66]. Devaraj S, Munichandraiah N, J. Phys. Chem. *C* 2008, 112, 4406.

[67]. Alfaruqi MH, Gim J, Kim S, Song J, Pham DT, Jo J, Xiu Z, Mathew V, Kim J, Electrochem. Commun. 2015, 60, 121.

[68]. Bhattacharjee S, Controlled Release J 2016, 235, 337.

[69]. Chowdhury I, Cwiertny DM, Walker SL, Environ. Sci. Technol. 2012, 46, 6968. [PubMed: 22455349]

[70]. Klaine SJ, Alvarez PJJ, Batley GE, Fernandes TF, Handy RD, Lyon DY, Mahendra S, McLaughlin MJ, Lead JR, Environ. Toxicol. Chem. 2008, 27, 1825. [PubMed: 19086204]

[71]. Bols NC, Dayeh VR, Lee LEJ, Schirmer K, in Biochem. Mol. Biol. Fishes, Elsevier, 2005, pp. 43–84.

[72]. Eskes C, Boström A-C, Bowe G, Coecke S, Hartung T, Hendriks G, Pamies D, Piton A, Rovida C, Toxicol. Vitro Int. J. Publ. Assoc. BIBRA 2017, 45, 272.

[73]. Gray EP, Coleman JG, Bednar AJ, Kennedy AJ, Ranville JF, Higgins CP, Environ. Sci. Technol. 2013, 47, 14315. [PubMed: 24218983]

[74]. Guaiquil VH, Farber CM, Golde DW, Vera JC, J. Biol. Chem. 1997, 272, 9915. [PubMed: 9092530]

[75]. Milligan JR, Nucleic Acids Res. 2003, 31, 6258. [PubMed: 14576314]

[76]. Berrill Alex, Biddlecombe Jamie, Bracewell Daniel, in Pept. Protein Deliv, Academic Press, London ; San Diego, CA, 2011, p. 26.

[77]. Forman HJ, Zhang H, Rinna A, Mol. Aspects Med. 2009, 30, 1. [PubMed: 18796312]

[78]. Biswas SK, Rahman I, Mol. Aspects Med. 2009, 30, 60. [PubMed: 18760298]
[79]. Couto N, Wood J, Barber J, Free Radic. Biol. Med. 2016, 95, 27. [PubMed: 26923386]
[80]. Poole LB, Free Radic. Biol. Med. 2015, 80, 148. [PubMed: 25433365]
[81]. Chou H-C, Chan H-L, Proteome Sci. 2014, 12, 2. [PubMed: 24405781]
[82]. Lin H, Chen Y, Shi J, Chem. Soc. Rev. 2018, 47, 1938. [PubMed: 29417106]
[83]. Evans DH, Piermarini PM, Choe KP, Physiol. Rev. 2005, 85, 97. [PubMed: 15618479]
[84]. Griffitt RJ, Hyndman K, Denslow ND, Barber DS, Toxicol. Sci. Off. J. Soc. Toxicol. 2009, 107, 404.
[85]. Scown TM, Santos EM, Johnston BD, Gaiser B, Baalousha M, Mitov S, Lead JR, Stone V, Fernandes TF, Jepson M, van Aerle R, Tyler CR, Toxicol. Sci. 2010, 115, 521. [PubMed: 20219766]
[86]. Nimmo IA, Spalding CM, Comp. Biochem. Physiol. Part B Comp. Biochem. 1985, 82, 91.
[87]. Eyckmans M, Celis N, Horemans N, Blust R, De Boeck G, Aquat. Toxicol. Amst. Neth. 2011, 103, 112.
[88]. Zhang H, Ji Z, Xia T, Meng H, Low-Kam C, Liu R, Pokhrel S, Lin S, Wang X, Liao Y-P, Wang M, Li L, Rallo R, Damoiseaux R, Telesca D, Mädler L, Cohen Y, Zink JI, Nel AE, ACS Nano 2012, 6, 4349. [PubMed: 22502734]
[89]. Herszage J, dos Santos Afonso M, Luther GW, Environ. Sci. Technol. 2003, 37, 3332. [PubMed: 12966978]
[90]. Khan Z, Kumar P, Kabir-ud-Din J Colloid Interface Sci. 2005, 290, 184.
[91]. Deng R, Xie X, Vendrell M, Chang Y-T, Liu X, J. Am. Chem. Soc. 2011, 133, 20168. [PubMed: 22107163]
[92]. Wen J, Lv Y, Xu Y, Zhang P, Li H, Chen X, Li X, Zhang L, Liu F, Zeng W, Sun S, Acta Biomater. 2019, 83, 359. [PubMed: 30414486]
[93]. Ishii T, Mann GE, Redox Biol. 2014, 2, 786. [PubMed: 25009780]
[94]. Wang Z, Zhang Y-J, Liu M, Peterson A, Hurt RH, Nanoscale 2017, 9, 5398. [PubMed: 28426079]
[95]. Sanchez VC, Jachak A, Hurt RH, Kane AB, Chem. Res. Toxicol. 2012, 25, 15. [PubMed: 21954945]
[96]. Geiser M, Aerosol Med J. Pulm. Drug Deliv. 2010, 23, 207.
[97]. Ma-Hock L, Strauss V, Treumann S, Küttler K, Wohlleben W, Hofmann T, Gröters S, Wiench K, van Ravenzwaay B, Landsiedel R, Part. Fibre Toxicol. 2013, 10, 23. [PubMed: 23773277]
[98]. Schinwald A, Murphy F, Askounis A, Koutsos V, Sefiane K, Donaldson K, Campbell CJ, Nanotoxicology 2014, 8, 824. [PubMed: 23924429]
[99]. Mao L, Hu M, Pan B, Xie Y, Petersen EJ, Part. Fibre Toxicol. 2015, 13, 7.
[100]. Schmid O, Möller W, Semmler-Behnke M, Ferron GA, Karg E, Lipka J, Schulz H, Kreyling WG, Stoeger T, Biomark. Biochem. Indic. Expo. Response Susceptibility Chem. 2009, 14 Suppl 1, 67.
[101]. Cantin AM, North SL, Hubbard RC, Crystal RG, J. Appl. Physiol. Bethesda Md 1985 1987, 63, 152.
[102]. Li Y, Yuan H, von dem Bussche A, Creighton M, Hurt RH, Kane AB, Gao H, Proc. Natl. Acad. Sci. 2013, 110, 12295. [PubMed: 23840061]
[103]. Oberdörster G, Elder A, Rinderknecht A, J. Nanosci. Nanotechnol. 2009, 9, 4996. [PubMed: 19928180]
[104]. van der Vliet A, O'Neill CA, Cross CE, Koostra JM, Volz WG, Halliwell B, Louie S, Am. J. Physiol. 1999, 276, L289. [PubMed: 9950891]
[105]. Andersen ME, Gearhart JM, Clewell HJ, Neurotoxicology 1999, 20, 161. [PubMed: 10385880]
[106]. Dorman DC, Struve MF, Clewell HJ, Andersen ME, Neurotoxicology 2006, 27, 752. [PubMed: 16644014]
[107]. Sunda WG, Huntsman SA, Harvey GR, Nature 1983, 301, 234.
[108]. Godtfredsen KL, Stone AT, Environ. Sci. Technol. 1994, 28, 1450. [PubMed: 22165928]
[109]. Evans DH, Environ. Health Perspect. 1987, 71, 47. [PubMed: 3297663]

[110]. VanWinkle B, de Mesy Bentley K, Malecki J, Gunter K, Evans I, Elder A, Finkelstein J, Oberdorster G, Gunter T, Nanotoxicology 2009, 1.

[111]. Hussain SM, Warheit DB, Ng SP, Comfort KK, Grabinski CM, Braydich-Stolle LK, Toxicol. Sci. Off. J. Soc. Toxicol. 2015, 147, 5.

[112]. Subramanian V, Zhu H, Wei B, Chem. Phys. Lett. 2008, 453, 242.

[113]. Shi S, Xu C, Yang C, Chen Y, Liu J, Kang F, Sci. Rep. 2013, 3, DOI 10.1038/srep02598.

[114]. Wei C, Yu L, Cui C, Lin J, Wei C, Mathews N, Huo F, Sritharan T, Xu Z, Chem. Commun. 2014, 50, 7885.

[115]. Lastoskie C, Gubbins KE, Quirke N, Langmuir 1993, 9, 2693.

[116]. del Pino P, Pelaz B, Zhang Q, Maffre P, Nienhaus GU, Parak WJ, Mater Horiz 2014, 1, 301.

[117]. Lee LEJ, Dayeh VR, Schirmer K, Bols NC, In Vitro Cell. Dev. Biol. Anim. 2009, 45, 127. [PubMed: 19184248]

[118]. Tanneberger K, Knöbel M, Busser FJM, Sinnige TL, Hermens JLM, Schirmer K, Environ. Sci. Technol. 2013, 47, 1110. [PubMed: 23227966]

[119]. Ferreira M, Costa J, Reis-Henriques MA, Front. Physiol. 2014, 5, 266. [PubMed: 25101003]

[120]. Luckenbach T, Fischer S, Sturm A, Comp. Biochem. Physiol. Part C Toxicol. Pharmacol 2014, 165, 28.

[121]. Schirmer K, Toxicology 2006, 224, 163. [PubMed: 16765501]

[122]. Creighton MA, Rangel-Mendez JR, Huang J, Kane AB, Hurt RH, Small 2013, 9, 1921. [PubMed: 25018686]

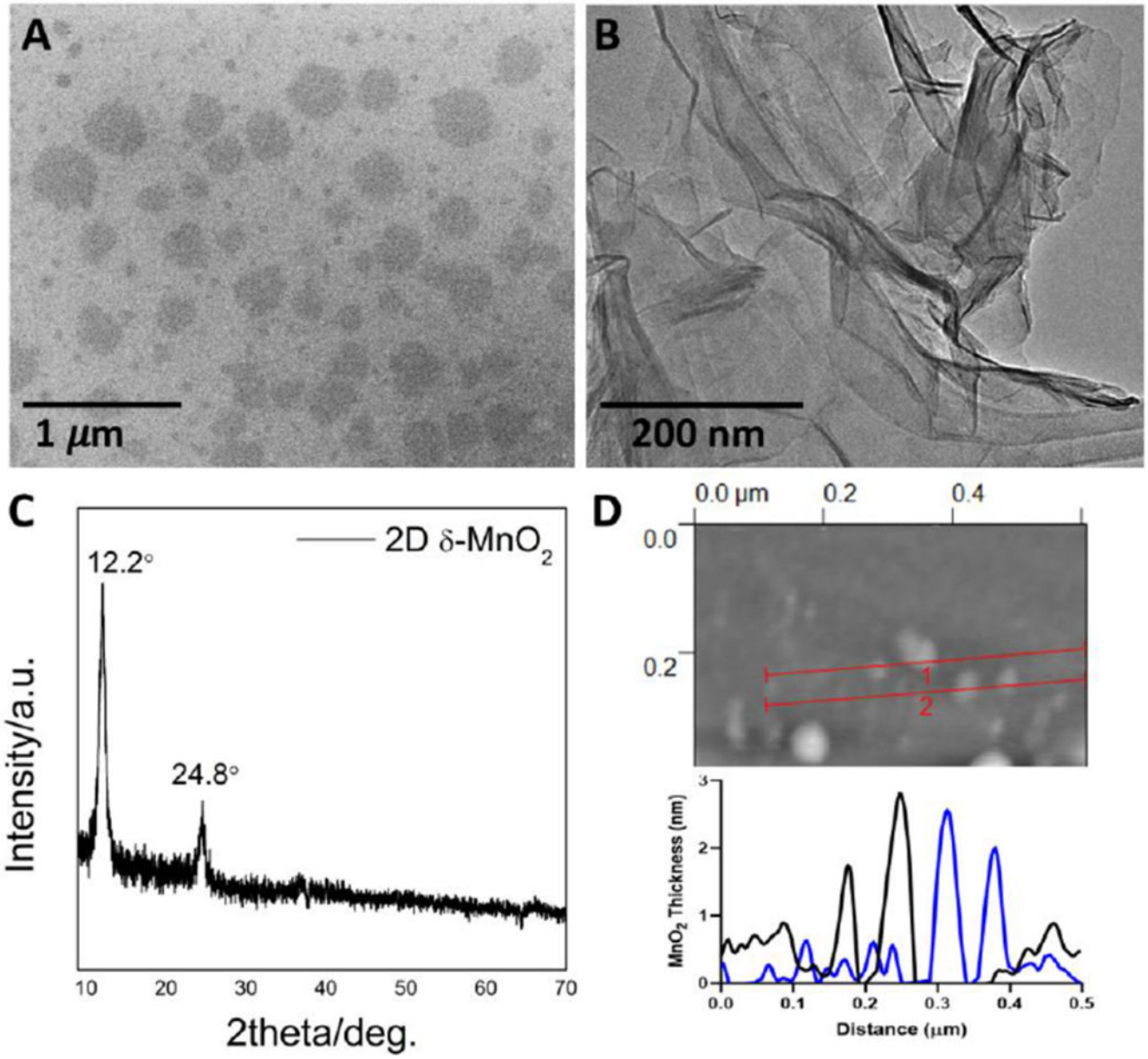

Figure 1.

MnO_2 nanosheet morphology and crystal phase. A. SEM image showing nanosheet lateral dimensions and in-plane shape/aspect-ratio; B. TEM image showing spontaneous wrinkling and folding that demonstrate nanosheet flexibility; C. X-ray diffractogram showing characteristic peaks for the layered 2D δ-phase; D. Atomic force microscope images with line profiles showing typical thicknesses of the monolayer and few-layer nanosheets.

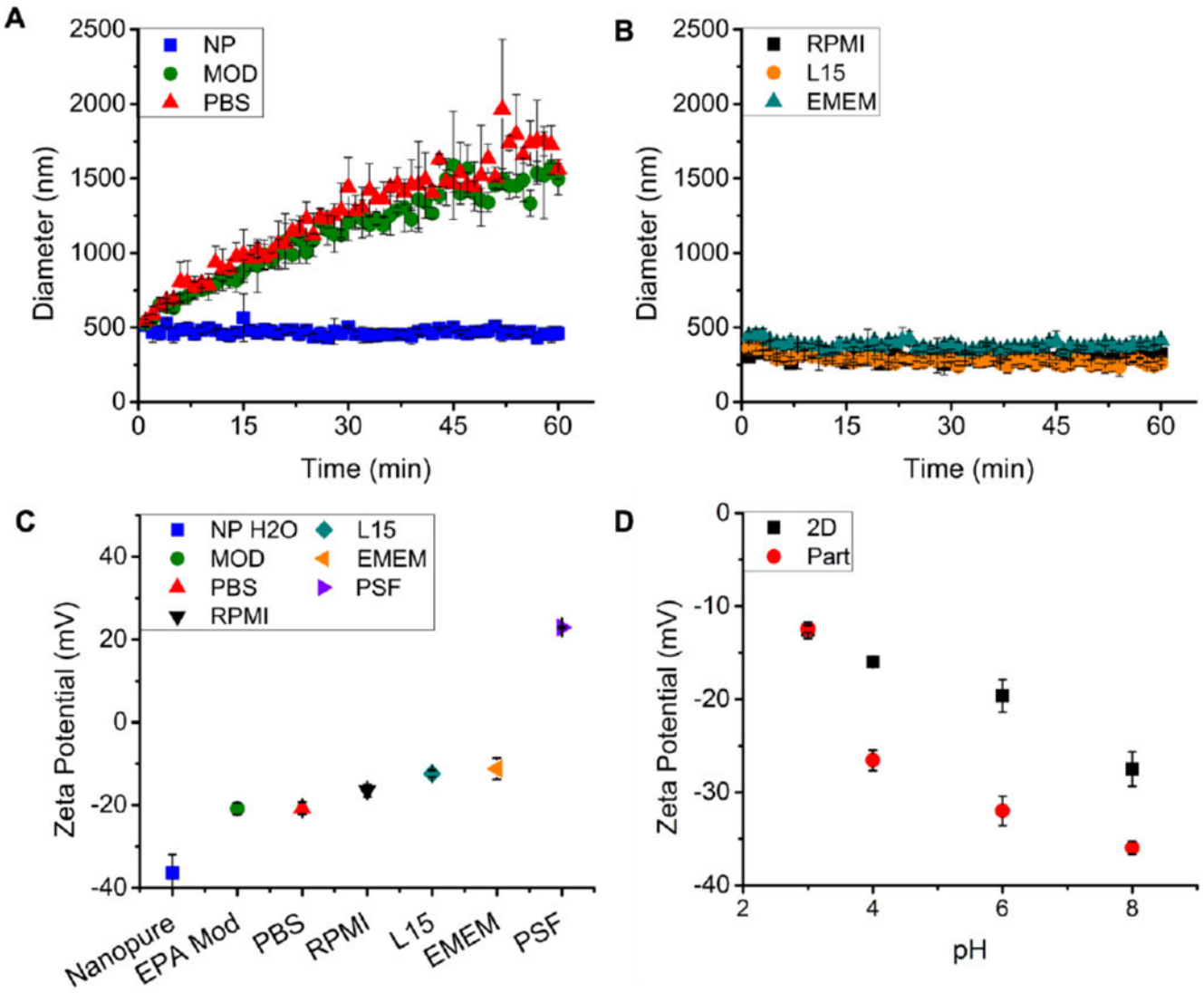

Figure 2.

Colloidal dynamics of MnO_2 nanosheets in aqueous media. A: Time-resolved DLS size measurements in simple media; B: Time-resolve DLS size measurements in cell culture media supplemented with fetal bovine serum; C: Zeta-potentials in simple and complex media; D: pH-dependent zeta potentials for MnO_2 nanosheets (2D) and reference particles (Part), using a series of buffers. Abbreviations for pH buffers are as follows. NP-nanopure water (nominally pH-7), MOD-EPA moderately hard water (pH-7.4-7.8), PBS-phosphate buffered saline (pH 7.4), RPMI-Roswell Park Memorial Institute medium (pH 7), L15-Leibovits's L15 medium (pH 7), EMEM-Eagle's Minimum Essential Medium (pH 7-7.4), PSF- phagolysosomal simulant fluid (pH 4.5).

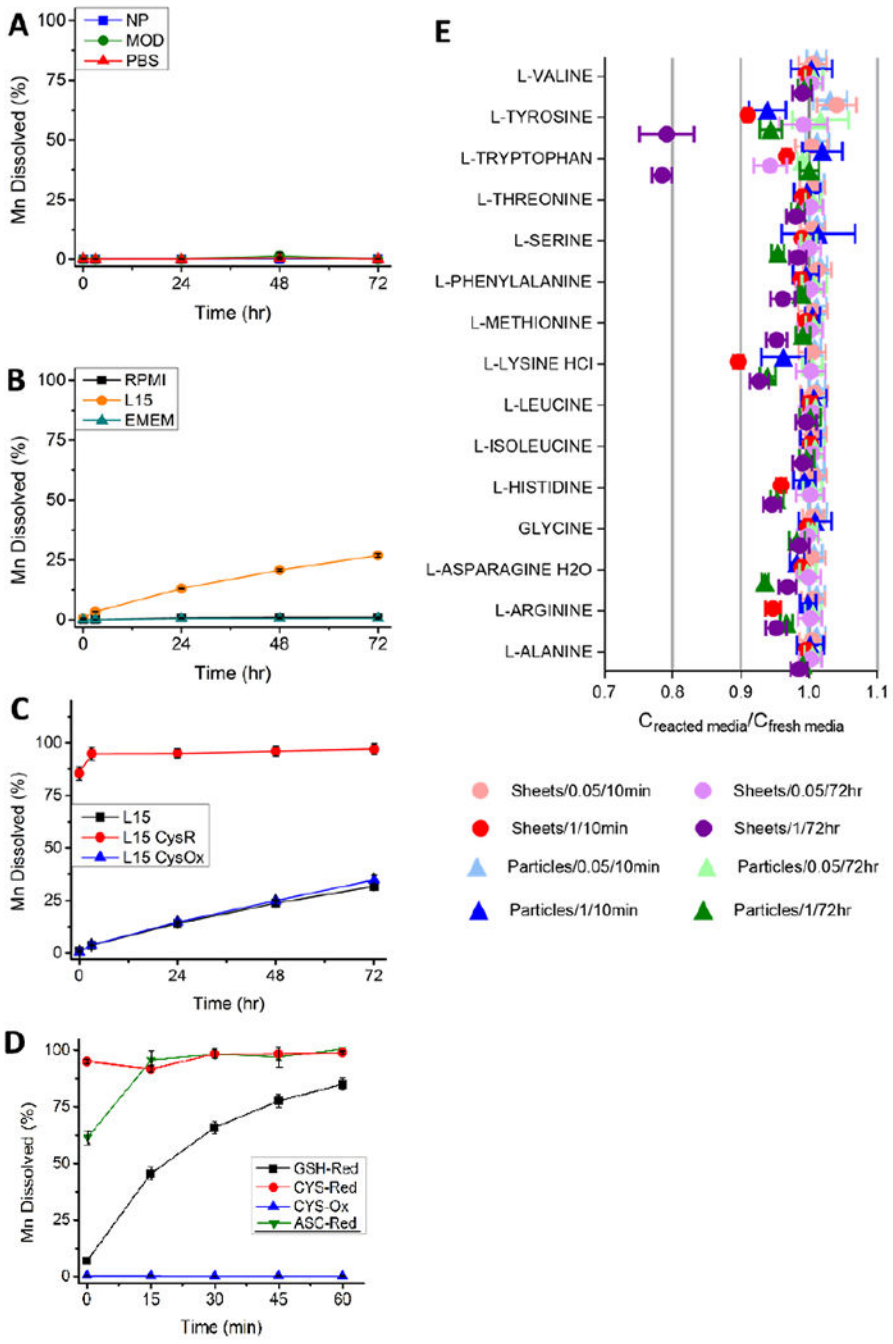

Figure 3.

Reductive dissolution kinetics of MnO_2 nanosheets in biological media relevant for safety assessment. A-D: Time-resolved dissolution percentages measured using ICP-AES analysis of dissolved total manganese following ultrafiltration (20 nm cutoff) removal of solids. A: No measurable dissolution in simple aqueous phases; B: Slow partial dissolution in L15 cell culture medium, but not in RPMI, EMEM. C: Rapid dissolution for L15 medium supplemented with 1 mM cysteine (reduced form. CysR), and no effect for addition of cystine (oxidized form, CysOx); D: Early time behavior (0-60 min) of reductive dissolution

in PBS buffer supplemented with 1 mM biological antioxidants cysteine, glutathione (GSH) and 0.5 mM ascorbate. Experiments in A-D used 8.69 mg/L solids addition with the exception of ascorbic acid which used 4.35 mg/L. ICP-AES instrumental detection limits were ~ 100 ppt. E: Analysis of 15 amino acids following acellular exposure of L15 cell culture medium to MnO_2 nanosheets ("Sheets") and reference particles ("Particles") at various solid concentrations (0.05 mg/ml; 1 mg/ml) and for various exposure times (10 min, 72 hr).

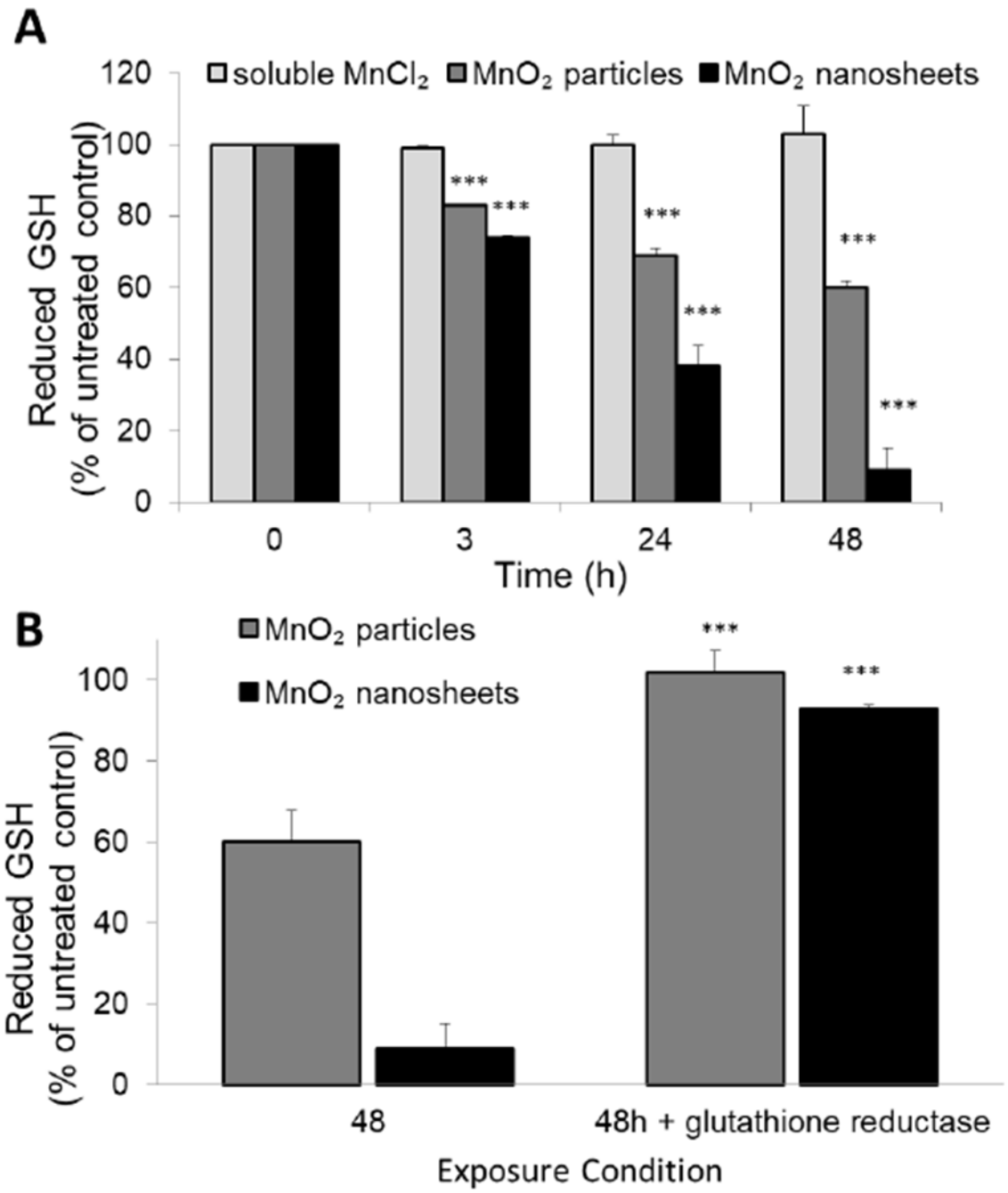

Figure 4.

MnO_2 nanosheets and particles cause acellular oxidation of GHS to GSSG. (A) Reduced glutathione (GSH) levels were significantly depleted after exposure to MnO_2 particles and nanosheets (***$p<0.0001$). MnO_2 nanosheets depleted GSH to a greater extent than MnO_2 particles or Mn^{2+} ions (no depletion). (B) GSH levels significantly recovered after the addition of the enzyme glutathione reductase and its cofactor NADPH, indicating that the MnO_2 / GSH reaction product was primarily GSSG (***$p<0.0001$; n=3).

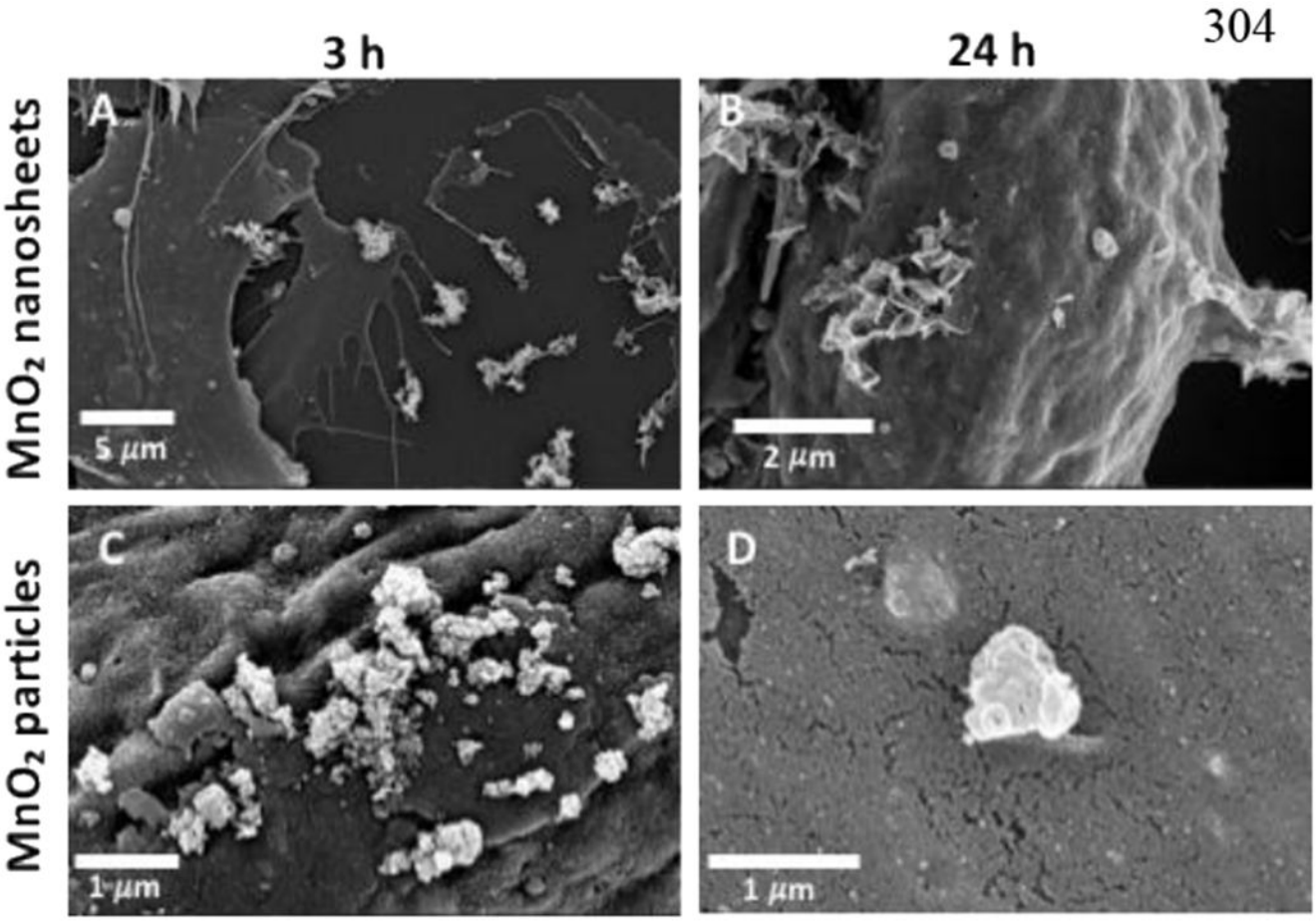

Figure 5.

MnO_2 nanosheets and particles survive in cell culture medium and interact with the cellular surface membrane of fish gill cells. SEM micrographs of MnO_2 nanosheets (A, B) and particles (C, D) interacting with cell membranes after 3 hr (A, C) and after 24 hr (B, D).

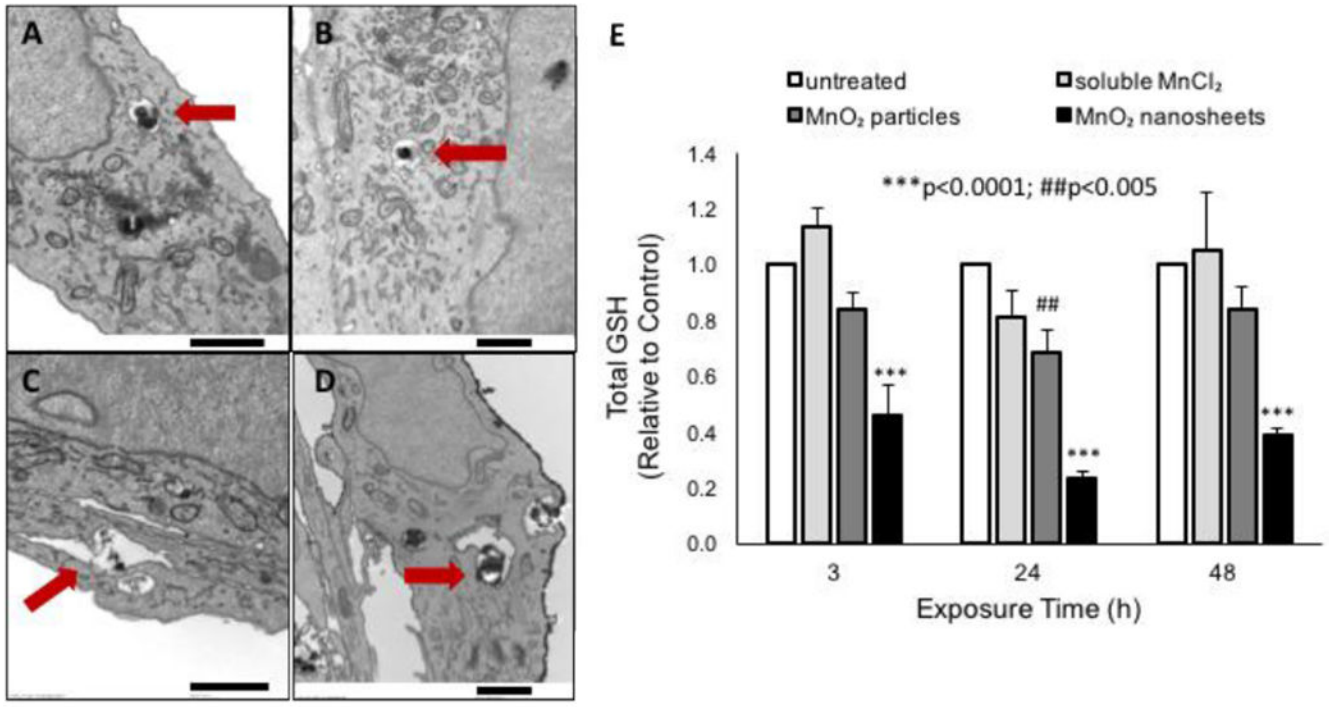

Figure 6.

Cell uptake of MnO_2 materials and effects on intracellular glutathione levels. A-D. MnO_2 nanosheets and particles are internalized by fish gill cells as intact solids, before dissolution. TEM micrographs of MnO_2 nanosheets (A, B) and particles (C, D) within intracellular vacuoles after 24 hr (A, C) and 48 hr (B, D) exposure to 8.7 ug/mL MnO_2. E. MnO_2 nanosheets deplete intracellular GSH levels to a greater extent than MnO_2 particles. Cells were treated with 10 ppm Mn ion equivalent (15.8 ug/mL MnO_2 nanosheets or particles). Scale bars: 1 μm.

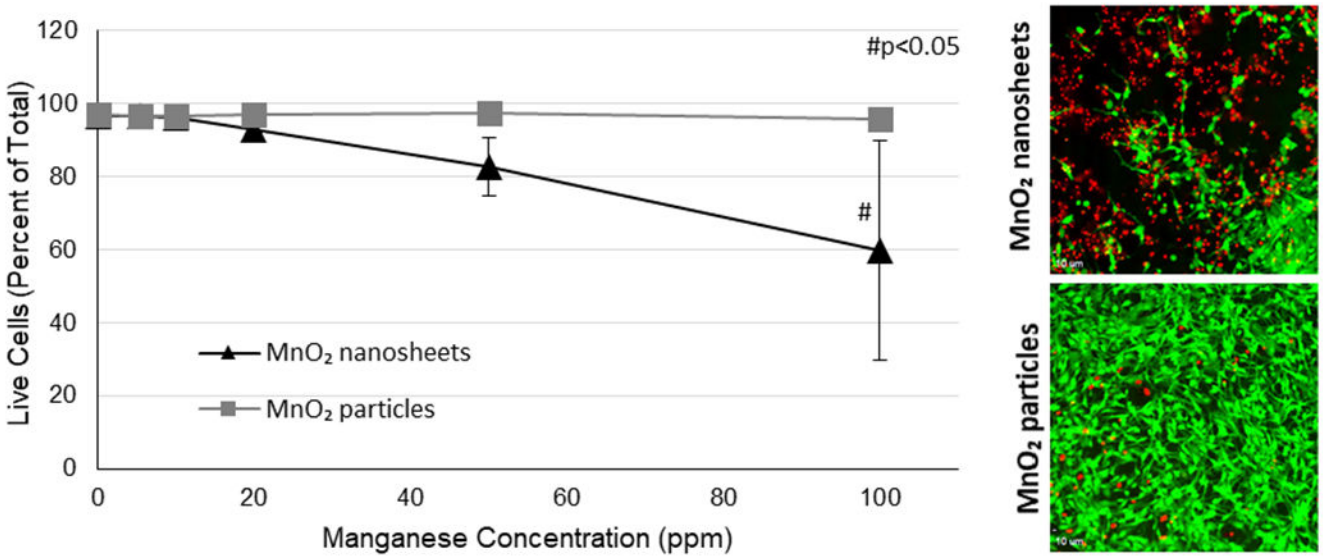

Figure 7.

Cytotoxicity of MnO_2 nanosheets and particles. Live cells were stained green with calcein AM and dead cells were stained red with ethidium homodimer 1. Cells were exposed to 5-100 ppm (8.7–158.2 ug/mL) MnO_2 nanosheets or particles for 72 h.